Applied Surface Science 644 (2024) 158784

Contents lists available at ScienceDirect

Applied Surface Science

journal homepage: www.elsevier.com/locate/apsusc

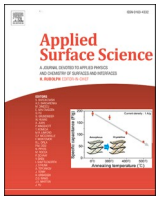

Full Length Article

Controlled laser-induced dehydrogenation of free-standing graphane probed by pump–probe X-ray photoemission

Roberto Costantini [a,b,*], Alessio Giampietri [c], Dario Marchiani [c], Maria Grazia Betti [c], Samuel Jeong [d], Yoshikazu Ito [d], Alberto Morgante [a,b], Martina Dell'Angela [b,*], Carlo Mariani [c,e,*]

[a] Dipartimento di Fisica, Università di Trieste, Via Valerio 2, I-34127 Trieste, Italy
[b] CNR-IOM, Strada Statale 14 – km 163.5, I-34149 Trieste, Italy
[c] Dipartimento di Fisica, Università di Roma "La Sapienza", Piazzale Aldo Moro 2, I-00185 Roma, Italy
[d] Institute of Applied Physics, Graduate School of Pure and Applied Sciences, University of Tsukuba, Tsukuba 305-8573, Japan
[e] INFN Sezione di Roma, Piazzale Aldo Moro 2, I-00185 Roma, Italy

ARTICLE INFO

Keywords:
Nanoporous Graphene
Graphane
Pump-Probe Spectroscopy
Time-resolved Spectroscopy
X-ray Photoelectron Spectroscopy

ABSTRACT

The effects of optical excitation on fully hydrogenated free-standing nanoporous graphene have been characterized by pump–probe X-ray photoemission spectroscopy. Hydrogenated graphene, known as graphane, is characterized by a sp^3 hybridization, which induces a sp^3 component in the C 1s core level whose intensity can be used to monitor the hydrogen content. Under optical excitation we observe a partial dehydrogenation of graphane, which we attribute to local laser-induced heating; such result allows us to estimate the thermal conductivity of the material, for which we found an upper limit of 0.2 W/(m K), four orders of magnitude smaller than that of graphene. Such stark difference, combined with the possibility of dehydrogenating the graphane substrate via laser exposure, may be exploited to engineer nanostructured heat conduction channels in organic and hybrid organic–inorganic devices. We then explored the sub-nanosecond dynamics of the C 1s core level, which displays a kinetic energy shift and a peak broadening with two different decay constants, 210 ps and 130 ps, respectively. We assign the former to surface photovoltage, and the latter to transient lattice heating.

1. Introduction

Chemical functionalization is a feasible way to tailor the electronic properties of graphene; in particular, by saturating the aromatic sp^2 bonds with atomic hydrogen for sp^3 bonds, it is possible to synthesize a semiconducting 2D hydrocarbon: graphane [1–2]. In addition to the experimentally observed opening of a band gap [3], the hydrogenation of graphene is also expected to modify its thermal conductivity, which may offer new possibilities for thermal energy harvesting and management in electronic devices [4]. Monolayer graphene possesses a thermal conductivity as high as 5000 W/(m K) [5–7], making it an ideal heat transport material; on the other hand, for graphane, depending on the hydrogen coverage and isomeric type, a reduction of more than one order of magnitude is expected [8–11]. Hydrogenation can thus be exploited to accurately tune the thermal conductivity of graphene, allowing to engineer insulating patterns inside a heat conducting template, for achieving efficient thermal rectification [12–13].

To date, reliable experimental assessments on the physical properties of graphane are however lacking, due to its challenging synthesis process. In fact, although a large variety of methods have been tested to incorporate atomic H in the graphene lattice [14–21], the samples were characterized by considerable density of structural defects and thermal instability, with hydrogen desorption temperatures well below 770 K [19–20,22]. To improve these, we used a high-quality and free-standing nanoporous graphene (NPG) [23–25] for the graphane template, and a low energy atomic hydrogen in-vacuum capillary as the source [26]. NPG samples are continuous turbostratic single and bilayer free-standing graphene with low density of defects and all the hallmarks of an ideal semi-metallic graphene [24–25]. Recently, we demonstrated thermally stable (up to 920 K) [27], structural defect free and highly hydrogenated graphane [3,27–30]. Our procedure enables a reliable synthesis of stable graphane samples, which are the ideal platforms to

* Corresponding authors.
E-mail addresses: roberto.costantini@units.it (R. Costantini), dellangela@iom.cnr.it (M. Dell'Angela), carlo.mariani@uniroma1.it (C. Mariani).

https://doi.org/10.1016/j.apsusc.2023.158784
Received 14 September 2023; Accepted 28 October 2023
Available online 29 October 2023

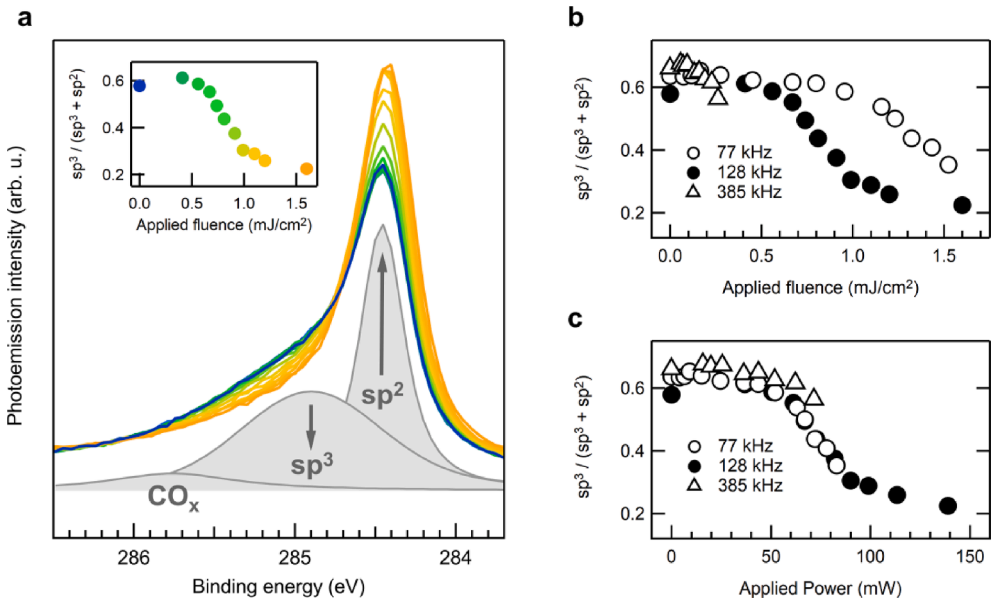

Fig. 1. (a) Evolution of the C 1s photoemission spectra of H-NPG under laser excitation at 128 kHz, acquired at a photon energy of 400 eV. The three different components used to fit the spectrum of the pristine sample (blue) are reported below the experimental curves. As indicated by the arrows, the increasing pump fluence leads to a visible reduction of the $sp^3/(sp^2 + sp^3)$ intensity ratio, which is also reported in the inset. The color of each circle matches that of the corresponding spectrum of the series. The $sp^3/(sp^2 + sp^3)$ ratio is reported for datasets acquired at different repetition rates as a function of the applied fluence (b) and power (c). The overlap of the data points in the latter case indicates that the observed effect is thermally activated.

experimentally measure the physical properties of the material.

In this paper, we use pump–probe X-ray photoemission spectroscopy (XPS) to characterize the response of free-standing hydrogenated-NPG to photoexcitation: the chemical selectivity of XPS allows us to resolve the sp^3 and sp^2 components in the C 1s spectra, and thus to monitor the hydrogen content as a function of the increasing laser fluence. By identifying the hydrogen desorption threshold, with aid of a theoretical model of pulsed laser local heating [31], we estimate a maximum value for the thermal conductivity of graphane of 0.2 W/(m K), which is 4 orders of magnitude smaller than that of graphene. Besides the chemical analysis, XPS may also provide information on phonon excitation and other many-body effects directly related to heat transport properties, which are detectable by analyzing the photoemission line shape. By exploiting the ~100 ps X-ray pulses delivered by the synchrotron, we thus analyze the excited state evolution in the sub-nanosecond range via time-resolved XPS, with the aim of observing the phonon dynamics of graphane. Our data show transient kinetic energy shift and broadening of the photoemission line with different decay rates, that we assigned to surface photovoltage effects and lattice heating, respectively.

2. Materials and methods

The fully freestanding NPG was obtained by a chemical vapor deposition (CVD) procedure at 1173 K using benzene as precursors, applied to a nanoporous Ni template. The latter was synthesized by using a $Ni_{30}Mn_{70}$ alloy sheet, etched with 0.5 M ammonium sulfate at 50 °C. Eventually, the bare NPG was obtained after 1.0 M hydrochloric acid treatment of the graphene-Ni template. Details and complete procedures for the NPG preparation and characterizations were reported elsewhere [23,32–36].

The NPG sample was thereafter mounted in an UHV chamber where it was annealed for a few hours at about 890 K, to let any residual contamination desorb from the graphene surface [28]. Atomic hydrogen was produced in the same UHV chamber by using a Focus GmbH apparatus, where a flux of the molecular gas is let flow through a capillary heated at about 2400 K by electron bombardment, thus obtaining more than 95% of the H atomic species [26], with an average energy of less than 0.2 eV. We exposed the NPG sample to 3600 L of atomic H (1 L = 1.33×10^{-6} mbar s), in a global chamber pressure of 1.0×10^{-6} mbar.

The so-obtained H-NPG sample has been first tested by using an XPS apparatus with a Mg Kα photon source (PSP TA10) and a hemispherical VG Microtech Clam-2 electron analyzer, used at constant pass energy (50 eV), with an overall energy resolution better than 1 eV. The estimated $sp^3/(sp^3 + sp^2)$ intensity ratio of the two main components in the C 1s spectrum results in about 60% of H:C uptake. After this calibration, the graphane sample has been dry-transferred to the Elettra synchrotron radiation facility (Italy) at the ANCHOR-SUNDYN endstation [37] of the ALOISA beamline. The transfer among laboratories of H-NPG with this method of hydrogenation has demonstrated not to modify the very stable H-C bond, only requiring a mild annealing (420 K) once in the new UHV apparatus, for getting rid of adventitious contamination.

Pump-probe XPS spectra were measured with laser and synchrotron beams impinging on the sample in a quasi-collinear geometry; the laser was focused to a diameter of 300 μm, which is a slightly larger spot size compared to the synchrotron probe. The fluence dependent data was acquired using the synchrotron multibunch radiation while illuminating the sample with the optical pump pulses. Such method allows for detecting irreversible modifications of the photoemission line shapes due to the laser excitation, and long-lived photo-induced effects with decay times at least comparable to the time between two consecutive laser pulses [38], which is 8 μs at a repetition rate of 128 kHz. The sub-nanosecond dynamics were instead probed using the hybrid mode filling of Elettra, acquiring only the electrons photoemitted by the isolated synchrotron pulses, as detailed in Ref. [39], and the pump–probe delay was scanned by an electronic phase shifter. The temporal resolution in such measurements was ~120 ps, as determined by the cross-correlation of pump (~300 fs) and probe (~120 ps) pulses.

3. Results and discussion

The effects of optical laser excitation on highly hydrogenated nanoporous graphene (H-NPG), have been monitored by X-ray photoelectron spectroscopy. A clear signature of the formation of C–H sp^3 bonds is the distinctive C 1s component observed at about 0.5 eV higher binding energy with respect to the well-known sp^2 peak of graphene

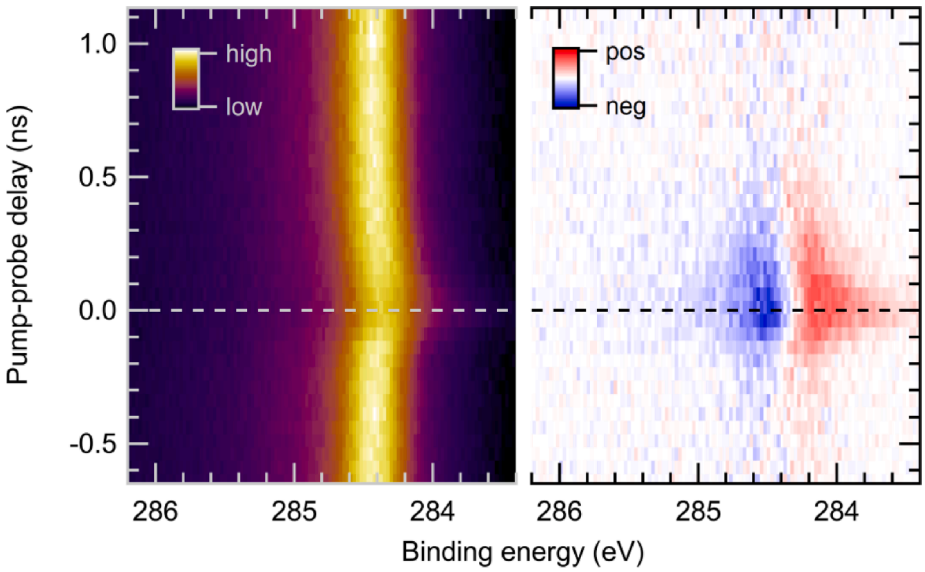

Fig. 2. False-color plot of the C 1s photoemission intensity as a function of binding energy and pump–probe delay, shown as raw data (left) and after subtraction of the unpumped reference (right). Significant energy shift and line broadening are observed around time zero. The applied fluence was 1.6 mJ/cm^2, at a repetition rate of 128 kHz.

[3,27–30]. The hydrogen coverage (θ) in at.% can be estimated by the intensity ratio among the two spectral components, namely $\theta = sp^3/(sp^3 + sp^2)$. In Fig. 1a, we show a series of C 1s XPS high-resolution spectra of highly hydrogenated graphene, acquired at a photon energy of 400 eV, as a function of the increasing laser fluence.

The blue spectrum represents the C 1s peak of the pristine H-NPG sample, prior to laser exposure, the green to orange spectra represent the C 1s peak at increasing laser fluence. All C 1s curves have been fitted after removing the Shirley background to reduce the number of fitting parameters involved. The C 1s peak is best fitted using three separate components found at binding energies of 284.5 eV, 285.0 eV and 285.8 eV, assigned to sp^2 and sp^3 coordinated C atoms, and to a minor contribution due to CO_x contamination, respectively. The sp^2 peak was fitted using a Doniach-Sunjic line shape, with an asymmetry associated to the expected semi-metallic nature of graphene [40]. To fit the sp^3 component a pseudo-Voigt line shape was used, namely a curve combining the intrinsic Lorentzian line shape of the excitation with a Gaussian response, the latter associated to the overall experimental resolution. The CO_x peak is fitted only with a Gaussian line shape, being associated to the convolution of different residual unresolved C-O bonds [27–29] and presenting however a small area in all spectra (below 6%).

Starting from a high initial hydrogen coverage ($\theta \approx 60\%$), we excited the H-NPG sample with laser pulses at a repetition rate of 128 kHz and at a wavelength of 515 nm (2.4 eV photon energy). As reported previously [41], we note irreversible changes in the C 1s line shape which occur immediately after laser exposure. In particular, the sp^3 component decreases in intensity, while most of the spectral density remains in the sp^2 peak. Such changes are enhanced at increasing laser fluence, and do not depend on the exposure time at a given fluence (*i.e.,* the relative distribution of components is stable in time under prolonged illumination). The spectral modifications are assigned to the local partial dehydrogenation of graphane, with θ decreasing from 60% to 20%, for a fluence of 1.6 mJ/cm^2, with an apparent threshold at about 0.75 mJ/cm^2, as shown in the inset to Fig. 1a. These results imply that laser exposure can be used to precisely etch graphitic channels with high thermal conductivity inside a graphane matrix with low thermal conductivity, which could prove useful for managing heat dissipation in nanoscale devices.

Analogous measurements have been performed on different areas of the pristine H-NPG sample, with the laser operated at 77 kHz and 385 kHz: the evolution of the hydrogen content (θ) is reported in Fig. 1b and 1c as a function of the applied laser fluence and power, respectively. The perfect overlap of the three datasets in the latter plot suggests that the dehydrogenation threshold is not related to the pulse energy, but is rather due to the local temperature increase. Indeed, it was observed that only annealing to 920 K causes a complete desorption of hydrogen in H-NPG, restoring the clean NPG template [27]. Electronically induced dehydrogenation has been predicted theoretically [42], although the high fluence used in the calculations (in the order of 10 mJ/cm^2) and the power-dependent decrease of θ as determined by our measurements, suggest to exclude such scenario as very origin of the induced dehydrogenation.

These observations can be used to evaluate the largely unknown thermal properties of graphane, based on the solution of the heat equations for pulsed laser excitation. After a large number of laser pulses, the system reaches a steady state and the sample base temperature increase (ΔT_{CW}) can be estimated as in the continuous wave (CW) regime [31]:

$$\Delta T_{CW} \approx \frac{P(1-R_c)}{2\sqrt{\pi}\, k\, w}, \tag{1}$$

where P is the impinging laser power, R_c is the reflection coefficient, k is the thermal diffusivity of the material, and w is the beam radius. The temperature increase therefore is directly proportional to $(1 - R_c)$, which accounts for the absorbance of the material, and is inversely proportional to the thermal diffusivity. To our knowledge, neither parameter has ever been determined experimentally for graphane. Based on our data, with $w = 150$ μm and a power of 75 mW, we can estimate the limits of the thermal diffusivity required for reaching ~920 K (*i.e.,* a temperature jump $\Delta T_{CW} \approx 650$ K from room temperature) necessary for the dehydrogenation. Depending on the graphane absorbance, the factor $(1 - R_c)$ may vary from 1 to 0.023 (the absorption of single layer graphene [43]). With these assumptions, we obtain a thermal diffusivity $0.005 < k < 0.2$ W/(m K). Theoretical models simulating heat transport in graphene flakes [44] and chemically functionalized graphene [8–9] indeed show that the thermal conductivity of the system may be strongly reduced with respect to the values $k > 1000$ W/(m K) experimentally reported for pure graphene [5–6]. Our experimental result is in qualitative agreement with the theoretical predictions, clearly bringing to light the reduction by orders of magnitudes of the thermal conductivity of graphane with respect to graphene.

The sub-nanosecond response of graphane to optical excitation has

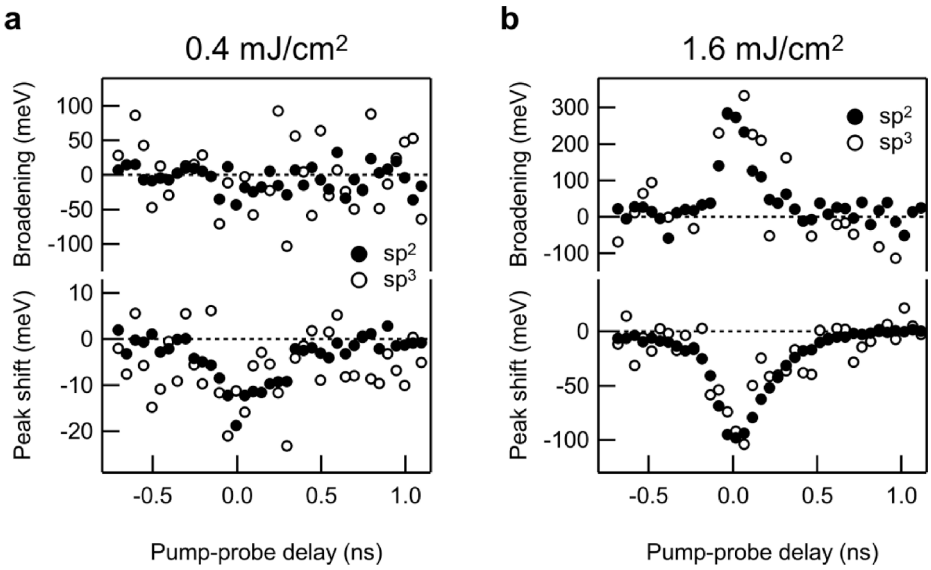

Fig. 3. Broadening and binding energy shift of sp^2 (closed circles) and sp^3 (open circles) components as extracted from the fits of C 1s spectra as a function of the pump–probe delay. At low fluence (a), shifts towards lower binding energies for both components are the only noticeable effects, while at high fluence (b) a significant peak broadening is also observed in addition to the shift.

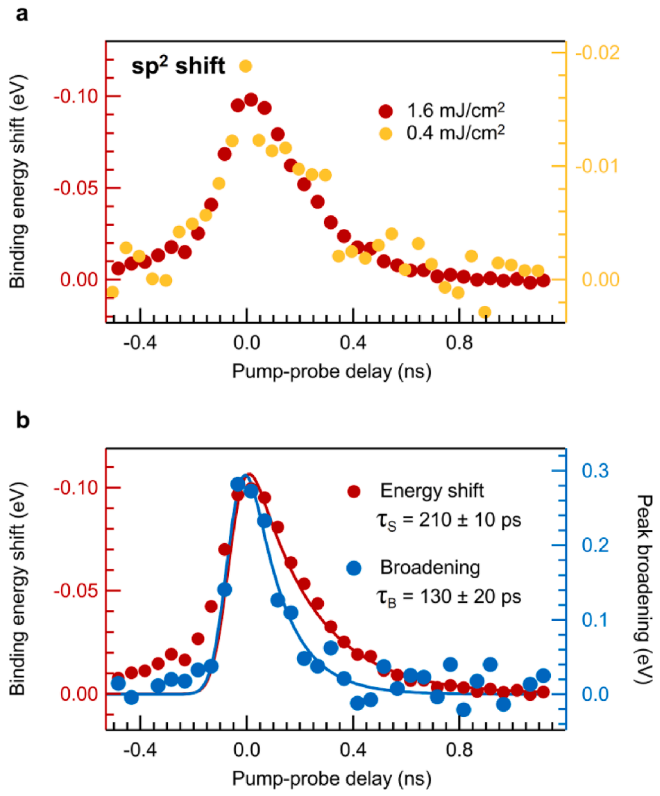

Fig. 4. (a) Comparison of energy shift for the 1.6 mJ/cm^2 (red, left axis) and 0.4 mJ/cm^2 (orange, right axis) measurements, showing that the dynamics of the effect are unchanged. (b) Shift (red, left axis) and broadening (blue, right axis) of the sp^2 component at 1.6 mJ/cm^2 fluence. Both trends have been fitted with exponentially modified Gaussian distributions (solid curves), obtaining time constants of 210 ± 10 ps for the energy shift and of 130 ± 20 ps for the broadening.

then been studied by time-resolved XPS, using a pump energy of 2.4 eV at a repetition rate of 128 kHz and probing the excited system with synchrotron pulses of 400 eV photon energy. Further experimental details are reported in the Materials and Methods section. We examined two excitation fluence regimes: 0.4 mJ/cm^2, below the dehydrogenation threshold, and 1.6 mJ/cm^2, when the hydrogen content is reduced to 20%. Fig. 2 shows the C 1s data in a false-color plot as a function of the pump–probe delay for the high fluence case. In the right panel, the signal after the subtraction of the unpumped spectra is also shown, to highlight the photo-induced effects.

A clear energy shift of 100 meV to lower binding energies and a spectral line broadening are observed around time zero, on a time scale shorter than 1 ns. The C 1s spectra at each delay time have been fitted to quantify such effects, and the obtained broadening and binding energy shift of the sp^2 and sp^3 peaks are reported in Fig. 3, for both the 0.4 mJ/cm^2 and 1.6 mJ/cm^2 fluences. At high fluence the energy shift is accompanied by a significant broadening of the photoemission line, while at low fluence only the spectral shift is observed. In both cases no significant difference is observed between the time-dependence of the sp^2 and sp^3 components.

It has to be reminded that while in the 0.4 mJ/cm^2 fluence regime (at 128 kHz) the hydrogen content is unaltered, with 1.6 mJ/cm^2 it is significantly reduced, meaning that the sample has a more graphenic character with respect to the pristine H-NPG; this implies that the thermal and electronic properties of the sample are irreversibly modified at the higher laser power. Nevertheless, a direct comparison of the energy shifts in the two cases, displayed in Fig. 4a, indicates that the dynamics are essentially unaltered. Rigid shifts of photoelectron spectra as the ones observed here are usually due to space charge [45–47] or surface photovoltage (SPV) [48–50] effects: the former is due to the cloud of low-energy electrons photoemitted by the pump pulse, while the latter is related to the transient electric field arising after exciton separation. The low pump-induced photoemission intensity in this experiment allows us to attribute the observed shift to SPV effects, which are expected considering the semiconducting character of the material [3]. Furthermore, the presence of SPV shifts at the higher fluence, suggests that the partially dehydrogenated sample retains its semiconducting properties.

In Fig. 4b we compare the dynamics of broadening and energy shift measured at 1.6 mJ/cm^2 fluence. The temporal dependence of shift (red circles, left axis) and broadening (blue circles, right axis) of the sp^2 component have been fitted with exponentially modified Gaussian distributions (solid lines). In particular, the Gaussian full width at half maximum (FWHM) was constrained to 120 ps to account for the

temporal resolution of the system, which was determined by the pump–probe cross correlation function, measured prior to the experiment. It readily emerges that the decay rates of broadening and shift are significantly different, with the fit yielding time constants $\tau_B = 130 \pm 20$ ps and $\tau_S = 210 \pm 10$ ps, respectively. Another clear difference is that while the exponentially modified Gaussian curve well reproduces the broadening dynamics in the whole temporal range, it does not correctly fit the shift at negative delay times: this has to be expected with transient SPV effects, in which the rising edge of the measured shift is related to the time of flight of the photoelectrons from the sample to the analyzer, rather than to the actual time constant of the SPV onset [51–52].

The origin of the broadening is instead less obvious, and its lifetime comparable to the probe pulse width prevents an unambiguous measurement of its decay. An analogous pump-induced broadening at the sub-picosecond time scale has been observed on the C 1s level of graphene [53], and was attributed to the high electronic temperature reached after photoexcitation. At a longer time scale only the phononic contribution is expected, although for a 300 meV broadening to be purely phonon-related a temperature of more than 3000 K is required [53–54]. Based on the observed dehydrogenation dependence on the average power rather than on the pulse energy, such high temperature seems overestimated. Nevertheless, it is not trivial to model heat dissipation in the partially dehydrogenated sample, which could present inhomogeneous domains with different electronic and thermal properties. In perspective, shorter probe pulses to examine the decay rates at higher temporal resolution, would allow a deeper understanding of the photo-induced dynamics of graphene.

4. Conclusions

We have shown that upon laser exposure with a suitable applied power (> 75 mW) a partial dehydrogenation of highly hydrogenated graphene can be triggered, which we ascribed to the local temperature increase, up to ~920 K. Our data point to a significant reduction of the thermal conductivity of graphane with respect to that of pristine graphene, from more than 1000 W/(m K) to less than 0.2 W/(m K), due to hydrogen functionalization. To our knowledge, this is the first experimental assessment of the thermal conductivity of free-standing hydrogenated graphene. Our experiments also suggest that laser-controlled hydrogen desorption on graphane may be used as a potential method for patterning heat conduction channels in nano-scale devices. Via time-resolved XPS, we have then characterized the photo-induced dynamics of graphane. We observed a transient energy shift and a line broadening which decay with two different time constants, 210 ps and 130 ps, that we attribute to surface photovoltage and lattice heating, respectively.

Funding Sources

This research was partially funded by PRIN 2017 FERMAT - 2017KFY7XF - CUP B54I1900117000 from Italian Ministry MUR, by Sapienza Ateneo funds and by JSPS KAKENHI (Grant Numbers JP21H02037, JP23K17661). This study was carried out within the National Quantum Science and Technology Institute (NQSTI) and received funding from the European Union Next-GenerationEU (PIANO NAZIONALE DI RIPRESA E RESILIENZA (PNRR) – MISSIONE 4 COMPONENTE 2, INVESTIMENTO 1.3 – PE_00000023).

CRediT authorship contribution statement

Roberto Costantini: Conceptualization, Investigation, Methodology, Writing – original draft. **Alessio Giampietri:** Investigation, Methodology. **Dario Marchiani:** Investigation, Methodology, Resources. **Maria Grazia Betti:** Conceptualization. **Samuel Jeong:** Resources. **Yoshikazu Ito:** Resources. **Alberto Morgante:** Investigation. **Martina Dell'Angela:** Conceptualization, Investigation, Methodology, Writing – original draft. **Carlo Mariani:** Conceptualization, Writing – original draft.

Declaration of Competing Interest

The authors declare that they have no known competing financial interests or personal relationships that could have appeared to influence the work reported in this paper.

Data availability

Data will be made available on request.

Acknowledgment

We kindly thank R. Mazzarello for the critical reading of the manuscript.

References

[1] J.O. Sofo, A.S. Chaudhari, G.D. Barber, Graphane: A Two-Dimensional Hydrocarbon, Phys. Rev. B 75 (15) (2007), 153401, https://doi.org/10.1103/PhysRevB.75.153401.
[2] P. Cudazzo, C. Attaccalite, I.V. Tokatly, A. Rubio, Strong Charge-Transfer Excitonic Effects and the Bose-Einstein Exciton Condensate in Graphane, Phys. Rev. Lett. 104 (22) (2010), 226804, https://doi.org/10.1103/PhysRevLett.104.226804.
[3] M.G. Betti, E. Placidi, C. Izzo, E. Blundo, A. Polimeni, M. Sbroscia, J. Avila, P. Dudin, K. Hu, Y. Ito, D. Prezzi, M. Bonacci, E. Molinari, C. Mariani, Gap Opening in Double-Sided Highly Hydrogenated Free-Standing Graphene, Nano Lett. 22 (7) (2022) 2971–2977, https://doi.org/10.1021/acs.nanolett.2c00162.
[4] Li, Y. T.; Tian, Y.; Sun, M. X.; Tu, T.; Ju, Z. Y.; Gou, G. Y.; Zhao, Y. F.; Yan, Z. Y.; Wu, F.; Xie, D.; Tian, H.; Yang, Y.; Ren, T. L. Graphene-Based Devices for Thermal Energy Conversion and Utilization. *Advanced Functional Materials*. Wiley-VCH Verlag February 1, 2020. 10.1002/adfm.201903888.
[5] A.A. Balandin, S. Ghosh, W. Bao, I. Calizo, D. Teweldebrhan, F. Miao, C.N. Lau, Superior Thermal Conductivity of Single-Layer Graphene, Nano Lett. 8 (3) (2008) 902–907, https://doi.org/10.1021/nl0731872.
[6] S. Chen, Q. Li, Q. Zhang, Y. Qu, H. Ji, R.S. Ruoff, W. Cai, Thermal Conductivity Measurements of Suspended Graphene with and without Wrinkles by Micro-Raman Mapping, Nanotechnology 23 (36) (2012), 365701, https://doi.org/10.1088/0957-4484/23/36/365701.
[7] S. Ghosh, I. Calizo, D. Teweldebrhan, E.P. Pokatilov, D.L. Nika, A.A. Balandin, W. Bao, F. Miao, C.N. Lau, Extremely High Thermal Conductivity of Graphene: Prospects for Thermal Management Applications in Nanoelectronic Circuits, Appl. Phys. Lett. 92 (15) (2008), https://doi.org/10.1063/1.2907977.
[8] S.-K. Chien, Y.-T. Yang, C.-K. Chen, Influence of Hydrogen Functionalization on Thermal Conductivity of Graphene: Nonequilibrium Molecular Dynamics Simulations, Appl. Phys. Lett. 98 (3) (2011), 033107, https://doi.org/10.1063/1.3543622.
[9] J.Y. Kim, J.-H. Lee, J.C. Grossman, Thermal Transport in Functionalized Graphene, ACS Nano 6 (10) (2012) 9050–9057, https://doi.org/10.1021/nn3031595.
[10] G. Barbarino, C. Melis, L. Colombo, Effect of Hydrogenation on Graphene Thermal Transport, Carbon N Y 80 (1) (2014) 167–173, https://doi.org/10.1016/j.carbon.2014.08.052.
[11] J. Chen, W. Ge, Computational Study on the Order-of-Magnitude Difference in Thermal Conductivity between Graphene and Graphane Nanoribbons, Diam. Relat. Mater. 129 (2022), 109335, https://doi.org/10.1016/j.diamond.2022.109335.
[12] C. Melis, G. Barbarino, L. Colombo, Exploiting Hydrogenation for Thermal Rectification in Graphene Nanoribbons, Phys. Rev. B 92 (24) (2015), 245408, https://doi.org/10.1103/PhysRevB.92.245408.
[13] Y. Li, A. Wei, D. Datta, Thermal Characteristics of Graphene Nanoribbons Endorsed by Surface Functionalization, Carbon N Y 113 (2017) 274–282, https://doi.org/10.1016/j.carbon.2016.11.067.
[14] D.C. Elias, R.R. Nair, T.M.G. Mohiuddin, S.V. Morozov, P. Blake, M.P. Halsall, A. C. Ferrari, D.W. Boukhvalov, M.I. Katsnelson, A.K. Geim, K.S. Novoselov, Control of Graphene's Properties by Reversible Hydrogenation: Evidence for Graphane, Science 323 (5914) (2009) 610–613, https://doi.org/10.1126/science.1167130.
[15] Z. Luo, J. Shang, S. Lim, D. Li, Q. Xiong, Z. Shen, J. Lin, T. Yu, Modulating the Electronic Structures of Graphene by Controllable Hydrogenation, Appl. Phys. Lett. 97 (23) (2010), 233111, https://doi.org/10.1063/1.3524217.
[16] J.S. Burgess, B.R. Matis, J.T. Robinson, F.A. Bulat, F. Keith Perkins, B.H. Houston, J.W. Baldwin, Tuning the Electronic Properties of Graphene by Hydrogenation in a Plasma Enhanced Chemical Vapor Deposition Reactor, Carbon N Y 49 (13) (2011) 4420–4426, https://doi.org/10.1016/j.carbon.2011.06.034.
[17] F. Zhao, Y. Raitses, X. Yang, A. Tan, C.G. Tully, High Hydrogen Coverage on Graphene via Low Temperature Plasma with Applied Magnetic Field, Carbon N Y 177 (2021) 244–251, https://doi.org/10.1016/j.carbon.2021.02.084.
[18] A. Paris, N. Verbitskiy, A. Nefedov, Y. Wang, A. Fedorov, D. Haberer, M. Oehzelt, L. Petaccia, D. Usachov, D. Vyalikh, H. Sachdev, C. Wöll, M. Knupfer, B. Büchner, L. Calliari, L. Yashina, S. Irle, A. Grüneis, Kinetic Isotope Effect in the

Hydrogenation and Deuteration of Graphene, Adv. Funct. Mater. 23 (13) (2013) 1628–1635, https://doi.org/10.1002/adfm.201202355.
[19] K.E. Whitener, W.K. Lee, P.M. Campbell, J.T. Robinson, P.E. Sheehan, Chemical Hydrogenation of Single-Layer Graphene Enables Completely Reversible Removal of Electrical Conductivity, Carbon N Y 72 (2014) 348–353, https://doi.org/10.1016/j.carbon.2014.02.022.
[20] J. Son, S. Lee, S.J. Kim, B.C. Park, H.-K. Lee, S. Kim, J.H. Kim, B.H. Hong, J. Hong, Hydrogenated Monolayer Graphene with Reversible and Tunable Wide Band Gap and Its Field-Effect Transistor, Nat. Commun. 7 (1) (2016) 13261, https://doi.org/10.1038/ncomms13261.
[21] M. Panahi, N. Solati, S. Kaya, Modifying Hydrogen Binding Strength of Graphene, Surf. Sci. 679 (2019) 24–30, https://doi.org/10.1016/j.susc.2018.08.009.
[22] Z. Luo, T. Yu, K. Kim, Z. Ni, Y. You, S. Lim, Z. Shen, S. Wang, J. Lin, Thickness-Dependent Reversible Hydrogenation of Graphene Layers, ACS Nano 3 (7) (2009) 1781–1788, https://doi.org/10.1021/nn900371t.
[23] Y. Ito, Y. Tanabe, H.-J. Qiu, K. Sugawara, S. Heguri, N.H. Tu, K.K. Huynh, T. Fujita, T. Takahashi, K. Tanigaki, M. Chen, High-Quality Three-Dimensional Nanoporous Graphene, Angew. Chem. Int. Ed. 53 (19) (2014) 4822–4826, https://doi.org/10.1002/anie.201402662.
[24] I. Di Bernardo, G. Avvisati, C. Mariani, N. Motta, C. Chen, J. Avila, M.C. Asensio, S. Lupi, Y. Ito, M. Chen, T. Fujita, M.G. Betti, Two-Dimensional Hallmark of Highly Interconnected Three-Dimensional Nanoporous Graphene, ACS Omega 2 (7) (2017) 3691–3697, https://doi.org/10.1021/acsomega.7b00706.
[25] I. Di Bernardo, G. Avvisati, C. Chen, J. Avila, M.C. Asensio, K. Hu, Y. Ito, P. Hines, J. Lipton-Duffin, L. Rintoul, N. Motta, C. Mariani, M.G. Betti, Topology and Doping Effects in Three-Dimensional Nanoporous Graphene, Carbon N Y 131 (2018) 258–265, https://doi.org/10.1016/j.carbon.2018.01.076.
[26] U. Bischler, E. Bertel, Simple Source of Atomic Hydrogen for Ultrahigh Vacuum Applications, J. Vac. Sci. Technol. A 11 (2) (1993) 458–460, https://doi.org/10.1116/1.578754.
[27] M.M.S. Abdelnabi, E. Blundo, M.G. Betti, G. Cavoto, E. Placidi, A. Polimeni, A. Ruocco, K. Hu, Y. Ito, C. Mariani, Towards Free-Standing Graphane: Atomic Hydrogen and Deuterium Bonding to Nano-Porous Graphene, Nanotechnology 32 (3) (2021), 035707, https://doi.org/10.1088/1361-6528/abbe56.
[28] M.M.S. Abdelnabi, C. Izzo, E. Blundo, M.G. Betti, M. Sbroscia, G. Di Bella, G. Cavoto, A. Polimeni, I. García-Cortés, I. Rucandio, A. Moroño, K. Hu, Y. Ito, C. Mariani, Deuterium Adsorption on Free-Standing Graphene, *Nanomaterials* 11 (1) (2021) 130, https://doi.org/10.3390/nano11010130.
[29] M.G. Betti, E. Blundo, M. De Luca, M. Felici, R. Frisenda, Y. Ito, S. Jeong, D. Marchiani, C. Mariani, A. Polimeni, M. Sbroscia, F. Trequattrini, R. Trotta, Homogeneous Spatial Distribution of Deuterium Chemisorbed on Free-Standing Graphene, Nanomaterials 12 (15) (2022) 2613, https://doi.org/10.3390/nano12152613.
[30] M.G. Betti, D. Marchiani, A. Tonelli, M. Sbroscia, E. Blundo, M. De Luca, A. Polimeni, R. Frisenda, C. Mariani, S. Jeong, Y. Ito, N. Cavani, R. Biagi, P.N. O. Gillespie, M.A. Hernandez Bertran, M. Bonacci, E. Molinari, V. De Renzi, D. Prezzi, Dielectric Response and Excitations of Hydrogenated Free-Standing Graphene, Carbon Trends 12 (2023), 100274, https://doi.org/10.1016/j.cartre.2023.100274.
[31] Y. Xu, R. Wang, S. Ma, L. Zhou, Y.R. Shen, C. Tian, Theoretical Analysis and Simulation of Pulsed Laser Heating at Interface, J. Appl. Phys. 123 (2) (2018), 025301, https://doi.org/10.1063/1.5008963.
[32] Y. Ito, W. Cong, T. Fujita, Z. Tang, M. Chen, High Catalytic Activity of Nitrogen and Sulfur Co-Doped Nanoporous Graphene in the Hydrogen Evolution Reaction, Angew. Chem. Int. Ed. 54 (7) (2015) 2131–2136, https://doi.org/10.1002/anie.201410050.
[33] Y. Ito, Y. Tanabe, J. Han, T. Fujita, K. Tanigaki, M. Chen, Multifunctional Porous Graphene for High-Efficiency Steam Generation by Heat Localization, Adv. Mater. 27 (29) (2015) 4302–4307, https://doi.org/10.1002/adma.201501832.
[34] Y. Ito, H.-J. Qiu, T. Fujita, Y. Tanabe, K. Tanigaki, M. Chen, Bicontinuous Nanoporous N-Doped Graphene for the Oxygen Reduction Reaction, Adv. Mater. 26 (24) (2014) 4145–4150, https://doi.org/10.1002/adma.201400570.
[35] Y. Tanabe, Y. Ito, K. Sugawara, M. Koshino, S. Kimura, T. Naito, I. Johnson, T. Takahashi, M. Chen, Dirac Fermion Kinetics in 3D Curved Graphene, Adv. Mater. 32 (48) (2020) 2005838, https://doi.org/10.1002/adma.202005838.
[36] Y. Tanabe, Y. Ito, K. Sugawara, D. Hojo, M. Koshino, T. Fujita, T. Aida, X. Xu, K. K. Huynh, H. Shimotani, T. Adschiri, T. Takahashi, K. Tanigaki, H. Aoki, M. Chen, Electric Properties of Dirac Fermions Captured into 3D Nanoporous Graphene Networks, Adv. Mater. 28 (46) (2016) 10304–10310, https://doi.org/10.1002/adma.201601067.
[37] R. Costantini, M. Stredansky, D. Cvetko, G. Kladnik, A. Verdini, P. Sigalotti, F. Cilento, F. Salvador, A. De Luisa, D. Benedetti, L. Floreano, A. Morgante, A. Cossaro, M. Dell'Angela, ANCHOR-SUNDYN: A Novel Endstation for Time Resolved Spectroscopy at the ALOISA Beamline, J Electron. Spectros. Relat. Phenomena 229 (2018) 7–12, https://doi.org/10.1016/j.elspec.2018.09.005.
[38] R. Costantini, F. Cilento, F. Salvador, A. Morgante, G. Giorgi, M. Palummo, M. Dell'Angela, Photo-Induced Lattice Distortion in 2H-MoTe 2 Probed by Time-Resolved Core Level Photoemission, Faraday Discuss. 236 (2022) 429–441, https://doi.org/10.1039/D1FD00105A.
[39] R. Costantini, R. Faber, A. Cossaro, L. Floreano, A. Verdini, C. Hättig, A. Morgante, S. Coriani, M. Dell'Angela, Picosecond Timescale Tracking of Pentacene Triplet Excitons with Chemical Sensitivity, Commun. Phys. 2 (1) (2019) 56, https://doi.org/10.1038/s42005-019-0157-1.
[40] P. Lacovig, M. Pozzo, D. Alfè, P. Vilmercati, A. Baraldi, S. Lizzit, Growth of Dome-Shaped Carbon Nanoislands on Ir(111): The Intermediate between Carbidic Clusters and Quasi-Free-Standing Graphene, Phys. Rev. Lett. 103 (16) (2009), 166101, https://doi.org/10.1103/PhysRevLett.103.166101.
[41] R. Costantini, D. Marchiani, M.G. Betti, C. Mariani, S. Jeong, Y. Ito, A. Morgante, M. Dell'Angela, Pump-Probe X-Ray Photoemission Spectroscopy of Free-Standing Graphane, Condens. Matter 8 (2) (2023) 31, https://doi.org/10.3390/condmat8020031.
[42] H. Zhang, Y. Miyamoto, A. Rubio, Laser-Induced Preferential Dehydrogenation of Graphane, Phys. Rev. B 85 (20) (2012), 201409, https://doi.org/10.1103/PhysRevB.85.201409.
[43] R.R. Nair, P. Blake, A.N. Grigorenko, K.S. Novoselov, T.J. Booth, T. Stauber, N.M. R. Peres, A.K. Geim, Fine Structure Constant Defines Visual Transparency of Graphene, Science 320 (5881) (2008) 1308, https://doi.org/10.1126/science.1156965.
[44] G. Fugallo, A. Cepellotti, L. Paulatto, M. Lazzeri, N. Marzari, F. Mauri, Thermal Conductivity of Graphene and Graphite: Collective Excitations and Mean Free Paths, Nano Lett. 14 (11) (2014) 6109–6114, https://doi.org/10.1021/nl502059f.
[45] S. Hellmann, K. Rossnagel, M. Marczynski-Bühlow, L. Kipp, Vacuum Space-Charge Effects in Solid-State Photoemission, Phys. Rev. B 79 (3) (2009), 035402, https://doi.org/10.1103/PhysRevB.79.035402.
[46] M. Dell'Angela, T. Anniyev, M. Beye, R. Coffee, A. Föhlisch, J. Gladh, S. Kaya, T. Katayama, O. Krupin, A. Nilsson, D. Nordlund, W.F. Schlotter, J.A. Sellberg, F. Sorgenfrei, J.J. Turner, H. Öström, H. Ogasawara, M. Wolf, W. Wurth, Vacuum Space Charge Effects in Sub-Picosecond Soft X-Ray Photoemission on a Molecular Adsorbate Layer, Struct. Dyn. 2 (2) (2015), 025101, https://doi.org/10.1063/1.4914892.
[47] G. Schiwietz, D. Kühn, A. Föhlisch, K. Holldack, T. Kachel, N. Pontius, Dynamics of Space-Charge Acceleration of X-Ray Generated Electrons Emitted from a Metal Surface, J Electron Spectros Relat Phenomena 220 (2017) 40–45, https://doi.org/10.1016/j.elspec.2017.03.003.
[48] W. Widdra, D. Bröcker, T. Gießel, I.V. Hertel, W. Krüger, A. Liero, F. Noack, V. Petrov, D. Pop, P.M. Schmidt, R. Weber, I. Will, B. Winter, Time-Resolved Core Level Photoemission: Surface Photovoltage Dynamics of the SiO2/Si(1 0 0) Interface, Surf. Sci. 543 (1–3) (2003) 87–94, https://doi.org/10.1016/J.SUSC.2003.07.005.
[49] B.F. Spencer, D.M. Graham, S.J.O. Hardman, E.A. Seddon, M.J. Cliffe, K.L. Syres, A. G. Thomas, S.K. Stubbs, F. Sirotti, M.G. Silly, P.F. Kirkham, A.R. Kumarasinghe, G. J. Hirst, A.J. Moss, S.F. Hill, D.A. Shaw, S. Chattopadhyay, W.R. Flavell, Time-Resolved Surface Photovoltage Measurements at n-Type Photovoltaic Surfaces: Si (111) and ZnO(101¯0), Phys. Rev. B 88 (19) (2013), 195301, https://doi.org/10.1103/PhysRevB.88.195301.
[50] K. Takahashi, S. Tokudomi, Y. Nagata, J. Azuma, M. Kamada, Surface Photo-Voltage Effect on Cr/GaAs(100) Studied by Photoemission Spectroscopy with the Combination of Synchrotron Radiation and Laser, J. Appl. Phys. 110 (11) (2011), https://doi.org/10.1063/1.3665214.
[51] S.-L. Yang, J.A. Sobota, P.S. Kirchmann, Z.-X. Shen, Electron Propagation from a Photo-Excited Surface: Implications for Time-Resolved Photoemission, Appl. Phys. A 116 (1) (2014) 85–90, https://doi.org/10.1007/s00339-013-8154-9.
[52] S. Tanaka, Utility and Constraint on the Use of Pump-Probe Photoelectron Spectroscopy for Detecting Time-Resolved Surface Photovoltage, J. Electron. Spectros. Relat. Phenomena 185 (5–7) (2012) 152–158, https://doi.org/10.1016/j.elspec.2012.06.003.
[53] D. Curcio, S. Pakdel, K. Volckaert, J.A. Miwa, S. Ulstrup, N. Lanatà, M. Bianchi, D. Kutnyakhov, F. Pressacco, G. Brenner, S. Dziarzhytski, H. Redlin, S.Y. Agustsson, K. Medjanik, D. Vasilyev, H.-J. Elmers, G. Schönhense, C. Tusche, Y.-J. Chen, F. Speck, T. Seyller, K. Bühlmann, R. Gort, F. Diekmann, K. Rossnagel, Y. Acremann, J. Demsar, W. Wurth, D. Lizzit, L. Bignardi, P. Lacovig, S. Lizzit, C. E. Sanders, P. Hofmann, Ultrafast Electronic Linewidth Broadening in the C 1s Core Level of Graphene, Phys. Rev. B 104 (16) (2021) L161104, https://doi.org/10.1103/PhysRevB.104.L161104.
[54] M. Pozzo, D. Alfè, P. Lacovig, P. Hofmann, S. Lizzit, A. Baraldi, Thermal Expansion of Supported and Freestanding Graphene: Lattice Constant versus Interatomic Distance, Phys. Rev. Lett. 106 (13) (2011), 135501, https://doi.org/10.1103/PhysRevLett.106.135501.